Numerical simulation of spacecraft re-entry non-equilibrium plasma flow based on collision-radiation model

Yao-Wen Du[1,2], Su-Rong Sun[1,3], Xian Meng[2], He-Ji Huang[2], Jin-Wen Cao[2], and Hai-Xing Wang[1,3]

[1] *School of Astronautics, Beihang University, Beijing, China*
[2] *Institute of Mechanics, Chinese Academy of Sciences, Beijing, China*
[3] *Ningbo Institute of Technology, Beihang University, Ningbo, China*

Abstract: A high-temperature air collisional-radiative model considering both vibrational and electronic states is established to investigate the plasma characteristics during earth reentry. The results show that there is a strong nonequilibrium effect in the post-shock plasma flow. The vibrational and electronic modes play critical roles on the energy transfer by excitations under heavy-particle impact and de-excitations under electron impact. The elastic collisions are also an important channel transfers energy from translational mode to electrons.

Keywords: Hypersonic, Air Plasma Flow, Collisional-Radiative model, Energy Relaxation

1. Introduction

With the rapid development of space exploration technology, the accurate prediction of thermal protection for atmospheric reentry vehicles has attracted widespread attention [1]. Compressed by the strong shock during the reentry into the atmosphere of Earth, the kinetic energy of gas is converted into the thermal energy, leading to the formation of a very high temperature environment around the vehicle, and usually results in an intense ablation of the surface. Under this condition, the thermal protection system is required to protect the safety for vehicle structure and carriers. Therefore, the key to the design of thermal protection system requires a detailed knowledge of the aerothermodynamics environment in the shock layer.

Efforts provided to solve the aerodynamic heating has been based on the coupling between flow equations and the thermochemical phenomena. The classic air global chemical models include the models developed by Park [2], Gupta [3], and Dung and Kang [4]. This kind of chemical model is very useful in the 2D or 3D flow calculations due to the relatively low computational cost. However, the populations of excited states could depart from the Boltzmann distribution in the shock layer as stated above, especially for the high-Height high-Mach reentry conditions [5].

Collisional-radiative models distinguish the different internal energy levels of species, and take into account all relevant collisional and radiative processes between them. However, due to the intensive computational cost, most calculations are performed in 0D model [6] or by coupling with the flow equations in 1D model [7, 8]. To our knowledge, the full electronic and vibrational CR model of air plasma coupled with the 1D flow model has not been proposed yet, thus in our study the air collisional-radiative model considering the detailed electronic and vibrational excited states is established to study the thermochemical characteristics behind shock wave by combining with the 1D flow model.

In this work, the vibrationally and electronic specific collisional-radiative model of air is developed, and the involved species and processes are described in Section 2. The description of the flow governing equations is also presented in Section 2. In Section 3, our model is validated by comparing with the experimental data. Then we focus our attention on the evolution of temperatures, excited states, and energy relaxation processes inside the post-shock high-temperature air plasmas at the flight height of 76.42 km and Mach number of 40.58 corresponding to the trajectory point t = 1634 s of FIRE (Flight Investigation of Reentry Environment) II. Finally, the conclusions are given in Section 4.

2. Mathematical model

2.1 High-temperature air collisional-radiative model

In this study, air is considered as a mixture of N_2 and O_2 and their products, which consists of molecules N_2, O_2, NO, atoms N, O, ions N_2^+, O_2^+, NO^+, N^+, O^+ and electrons. For the electronic ground state of N_2 and O_2, the 68 vibrational state of $N_2(X^1\Sigma_g^+)$ and 47 vibrational states of $O_2(X^3\Sigma_g^-)$ are taken into account in the model. The electronic excited states of N_2 and O_2 are also considered without differentiating the vibrational states. The electronic excited states of NO, N_2^+, O_2^+, and NO^+ are considered. For the atoms N and O, the model involves 46 electronic states of N and 40 electronic states of O in order to reasonably predict the ionization of N and O atoms. Only the electronic ground state has been considered for atomic ions N^+ and O^+. Table 1 lists the chemical species involved in the CR model, consisting of 248 states and electron.

The high-temperature air collisional-radiative model considers the collisional processes and radiative processes between particles in detail, including the vibrational excitation under the collision of electrons or heavy particles, the vibrational dissociation of molecules, the molecular electronic excitation, molecular ionization, atomic electronic excitation and ionization, excitation transfer between excited particles, etc. According to the detailed balance principle, the inverse rate coefficient was calculated by equilibrium constants. The model contained about 40,000 forward and inverse collisional processes. The detailed processes in the model can be found in [9].

Table 1. Species and states involved in CR model.

Types	Species	States
Molecules	N_2	$X^1\Sigma_g^+$ (v=0 → 67), $A^3\Sigma_u^+$, $B^3\Pi_g$, $W^3\Delta_u$, $B'^3\Sigma_u^-$, $a'\ ^1\Sigma_u^-$, $a^1\Pi_g$, $w^1\Delta_u$, $G^3\Delta_g$, $C^3\Pi_u$, $E^3\Sigma_g^+$
	O_2	$X^3\Sigma_g^-$ (v=0 → 46), $a^1\Delta_g$, $b^1\Sigma_g^+$, $c^1\Sigma_u^-$, $A'\ ^3\Delta_u$, $A^3\Sigma_u^+$, $B^3\Sigma_u^-$, $f^1\Sigma_u^+$
	NO	$X^2\Pi$, $a^4\Pi$, $A^2\Sigma^+$, $B^2\Pi$, $b^4\Sigma^-$, $C^2\Pi$, $D^2\Sigma^+$, $B'\ ^2\Delta$, $E^2\Sigma^+$, $F^2\Delta$
Molecular ions	N_2^+	$X^2\Sigma_g^+$, $A^2\Pi_u$, $B^2\Sigma_u^+$, $a^4\Sigma_u^+$, $D^2\Pi_g$, $C^2\Sigma_u^+$
	O_2^+	$X^2\Pi_g$, $a^4\Pi_u$, $A^2\Pi_u$, $b^4\Sigma_g^-$
	NO^+	$X^1\Sigma^+$, $a^3\Sigma^+$, $b^3\Pi$, $W^3\Delta$, $b'\ ^3\Sigma^-$, $A'\ ^1\Sigma^+$, $W^1\Delta$, $A^1\Pi$
Atoms	N	$^4S^0$, ^2D, ^2P, . . . (46 levels)
	O	^3P, ^1D, ^1S, . . . (40 levels)
Atomic ions	N^+	^3P
	O^+	$^4S^0$
Electron	e^-	-

2.2 Governing equations

In order to describe the plasma characteristics evolution along the stagnation-line during the reentry flight of vehicle, the 1D flow model combined with the above collisional-radiative model is established to simulate the plasma flow. Fig. 1. shows a 1D schematic picture of the flow behind a normal shock indicating the computational domain (x > 0) used in the study. Then the downstream plasma characteristics behind shock wave are solved by the conservation equations coupling with the CR model.

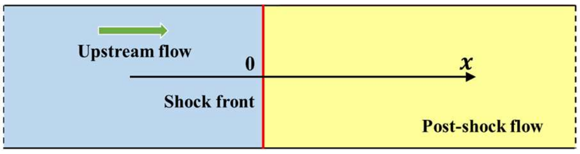

Fig. 1. Schematic picture of the flow behind shock front.

The conservation equation is as follows:

$$\frac{d}{dx}\left(\rho_{X_i} u\right) = M_{X_i}\left(\dot{\omega}_{X_i,C} + \dot{\omega}_{X_i,R}\right) \quad (1)$$

where u is the gas velocity, ρ_{X_i} is the mass density of X_i, and M_{X_i} is the mass of X_i. $\dot{\omega}_{X_i,C}$ and $\dot{\omega}_{X_i,R}$ are the collision and radiation source term. The momentum equation:

$$\frac{d}{dx}\left(\rho u^2 + p\right) = 0 \quad (2)$$

where ρ is the total density and p is the pressure. The pressure p is obtained from the equation of state. The energy balance equation of heavy species:

$$\frac{d}{dx}\left[u\left(e_{t,H} + e_{r,H} + p_H + \rho_H \frac{u^2}{2}\right)\right] = Q_{eH,elas} + Q_{H,inelas} \quad (3)$$

where $e_{t,H}$ is the translational energy of heavy species, $e_{r,H}$ is the rotational energy of heavy species, and ρ_H is the total density of the heavy species. $Q_{eH,elas}$ and $Q_{H,inelas}$ are the energy source terms due to the elastic and inelastic collisions, respectively. The electron energy equation:

$$\frac{d}{dx}\left[u\left(e_e + p_e + \rho_e \frac{u^2}{2}\right)\right] = -Q_{eH,elas} + Q_{e,inelas} \quad (4)$$

where e_e is the internal energy of electron, ρ_e is the mass density of electron, and $Q_{e,inelas}$ is the electron energy source term caused by inelastic collisions.

3. Numerical results

3.1 Model Validation

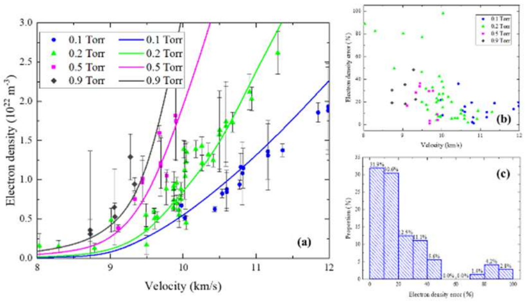

Fig. 2. Comparison between our calculated (line) and Cruden's measured (symbols) electron number density.

A comparison with measured electron density from Cruden et al. [10] is carried out to further validate our model. Cruden et al. measured the electron density behind the normal shock produced in the Electric Arc Shock Tube. Fig. 2(a) presents the comparison of our calculated electron density with Cruden's measured results versus shock wave velocity at the pressures of 0.1 Torr, 0.2 Torr, 0.5 Torr and 0.9 Torr. A good agreement is observed in Fig. 2(a). According to the error analysis in Fig. 2(b) and Fig. 2(c), more than 62% of data have a relative error of less than 20%. And this comparison would be better if errors in the experimental data were taken into account, which can be seen from the error bar in Fig. 2(a). This error analysis indicates the reasonable agreement between our calculated results and Cruden's experimental data, proving that our model has ability to predict the physicochemical characteristics of plasma flow behind the shock front.

3.2 Non-equilibrium energy transfer of plasma flow

In this section, our calculation is carried out for the elapsed time 1634 s from the launch, which corresponds to the height of 76.42 km and Mach number of 40.58. Fig. 3. presents the spatial evolution of characteristic temperatures in the post-shock plasma flow. As exhibited in Fig. 3., just behind the shock, T_{tr} becomes very high up to 62600 K, but T_e and T_{vib} are still very low. T_{N_2-vib} and T_{O_2-vib} start to increase slowly at x = 3×10^{-6} m, and reach the maximum of 15360 K and 20100 K at x = 4×10^{-4} m and x = 6×10^{-4} m respectively. Meanwhile, an obvious decrease in T_{tr} is clearly seen. After the peak value of vibrational temperature, both T_{tr} and T_{vib} undergo a strong decrease due to the energy loss caused by the molecular dissociation processes. The profile of T_e begins to rise at the position x = 4×10^{-4} m, and progressively has the same value with T_{N_2-vib} at x = 5×10^{-3} m, and finally reaches equilibrium with T_{tr} at x = 3×10^{-2} m. Under the impact of collisions, the flow reaches an equilibrium temperature equal to 10490 K. This indicates that the plasma achieves the thermal equilibrium at the distance of 30 mm from the shock front.

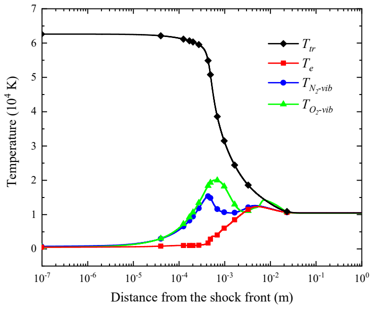

Fig. 3. The spatial evolution of temperatures.

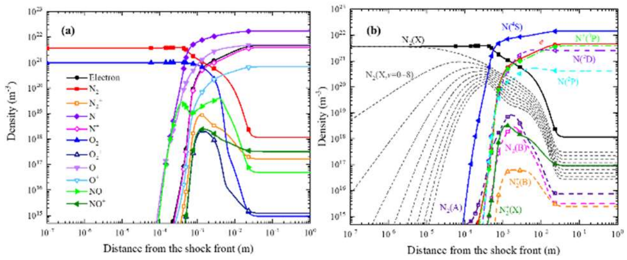

Fig. 4. The distribution of total species number density (a) and different excited states density (b) in the plasma flow.

Fig. 4(a) presents the evolution of species densities in the plasma flow. N and O rise rapidly from 0.1 mm due to the dissociation of N_2 and O_2. In the range from 0.1 mm to 1 mm, the dissociation degree rises from 2.2×10^{-7} to 0.8. Dissociation phase is immediately followed by the ionization phase. From 0.2 mm, the charged particles obviously increase. At the positions larger than 30 mm, the densities remain unchanged. Fig. 4(b) shows the evolution of the vibrational states of $N_2(X)$, electronic states of N_2, N_2^+ and N atom, N^+, and e. Behind the shock, the number densities of vibrational states first increase to high-lying levels due to the vibrational climb processes under heavy-particle impact. Then the vibrational distribution becomes concentrated at the position of about 0.1 mm, after this position, the vibrational states decrease rapidly because of the occurrence of dissociation processes, leading to the sharp rise of the number density of atoms $N(^4S)$. At the beginning stage in Fig. 4(b), atoms are mainly in the electronic ground state. These ground state atoms are excited by impact under electrons and heavy particles, the densities of excited states exhibit a fast increase.

In order to understand these parameters evolutions, the energy transfers between different internal energy modes are discussed in detail. Fig. 5. shows the contributions of different processes to the translational-rotational energy. In Eq. (3), the energy source terms include the elastic and inelastic collisions. Before the distance of 2×10^{-4} m, the dominant processes are the vibrational excitation processes.

$$N_2(X,v)+M \rightarrow N_2(X,v+1)+M$$

From 2×10^{-4} m to 2×10^{-3} m, there are several prominent peaks, among which the most obvious one is the vibrational dissociation of nitrogen under atomic impact.

$$N_2(X,v)+A \rightarrow N(^4S)+N(^4S)+A$$

Moreover, another important peak is caused by the neutral exchange reactions.

$$O_2(X,v)+N \leftrightarrow NO+O$$

In the final phase of energy relaxation, the energy loss caused by the N atomic excitation processes under heavy-particle impact exhibits a peak value at about 1 mm position from the shock front, and thus the N atomic excitation processes become the main energy loss mechanism after its maximum value.

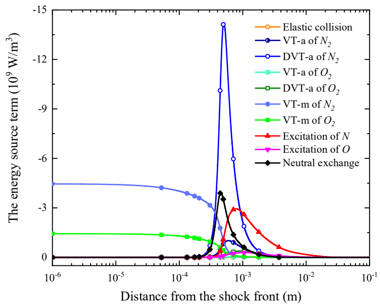

Fig. 5. The contributions of different processes to the translational-rotational energy.

Fig. 6. presents the contributions of different processes to the electron energy. Before the distance of 0.3 mm, the main processes leading to the electron energy gain are the vibrational de-excitation processes under electron impact.

$$N_2(X,v)+e \rightarrow N_2(X,w<v)+e$$

Beyond the distance of 0.3 mm, the de-excitation processes of excited N atoms under electron impact

$$N(j)+e \rightarrow N(i<j)+e$$

transfer a massive excitation energy to electrons. At the same time, the molecular vibrational de-excitation and elastic collisions also make obvious contributions to the rise of electron energy. Meanwhile, it can be noted that the ionization of atoms is the main electron energy loss channel. Afterwards, the elastic collisions become the main contribution to the increase in electron energy.

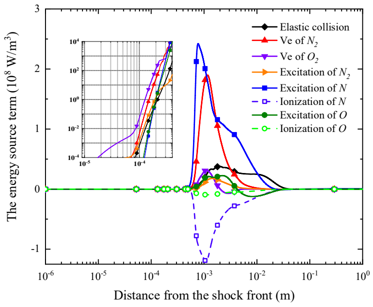

Fig. 6. The contributions of processes to electron.

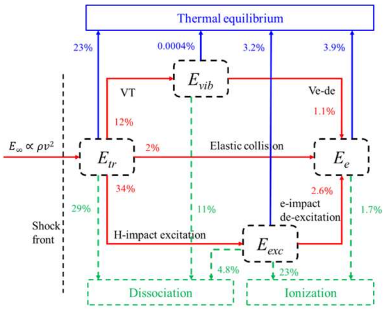

Fig. 7. The energy relaxation processes in plasma flow.

According to the above analysis, the energy relaxation in the post-shock flow is summarized in Fig. 7. Under the compression of shock wave, the kinetic energy is transformed into translational energy of molecules. Thereafter, the vibrational excitation processes under heavy-particle impact transfer part of the translational-rotational energy to the vibrational mode. After this accumulation, the vibrational de-excitation processes under electron impact release a large amount of vibrational energy to electrons. Moreover, the atoms are excited to high-lying states by heavy-particle impact, along with the energy gain from the translational-rotational mode. Then, the de-excitation processes of excited state atoms by electron impact result in the energy transfer to electrons. For the increase of electron energy, the above two paths are the dominant energy sources, comparable to the contribution of elastic collisions. This further provides evidence that the vibrational and electronic excited modes are critical for energy relaxation. In addition, except for the energy transfer, the total energy of flow is largely lost due to the dissociation and ionization processes, the dissociation processes mainly cause the loss of translational-rotational energy and vibrational energy, while the ionization processes lead to the loss of electronic excited and electron energy. The energy losses due to dissociation and ionization can be up to 70% of the total energy.

4. Conclusion

The high-temperature air collisional-radiative model coupled with one-dimensional flow governing equations is established to investigate the thermochemical non-equilibrium and energy relaxation in the post-shock plasma flow during earth reentry. In order to validate our model, the electron density is compared with experimental values, and the reasonable agreement is obtained.

The evolution of characteristics temperatures and chemical components in the post-shock stagnation-line plasma flow is analyzed in detail for the trajectory point 1634 s of FIRE II. The thickness of thermochemical non-equilibrium region is on the order of centimeter, which is comparable to the shock layer thickness, indicating that there is a strong non-equilibrium effect in the post-shock flow. The vibrational and electronic excited modes are critical to the energy transfer. The vibrational excitation processes under heavy-particle impact can transfer the translational energy to the vibrational mode, then the vibrational energy is transferred to electrons by the vibrational de-excitation processes under electron impact. The excitation of atoms by heavy-particle impact can gain energy from the translational mode, and the de-excitation processes of high-lying excited states under electron impact result in the energy transfer to electrons. Finally, the elastic collision between electrons and heavy particles is also an important channel that directly transfers energy from translational mode to electrons in the final stage.

5. Acknowledgements

We acknowledge financial support by the National Natural Science Foundation of China (Grant Numbers 11735004, 12005010) and State Key Laboratory of High Temperature Gas Dynamics (Grant Numbers 2021KF08).

6. References

[1] O. Uyanna, H. Najafi, Acta Astronautica, 176 (2020).
[2] C. Park, Journal of Thermophysics and Heat Transfer, 7 (1993).
[3] R.N. Gupta, J.M. Yos, NASA RP-1232, (1990).
[4] M.G. Dunn, NASA Contract. Reports, (1973).
[5] C. Park, Journal of Thermophysics and Heat Transfer, 20 (2006).
[6] A. Bultel, Physics of Plasmas, 13 (2006).
[7] M. Panesi, Journal of Thermophysics and Heat Transfer, 23 (2009).
[8] J. Annaloro, Journal of Thermophysics and Heat Transfer, 28 (2014).
[9] Y.W. Du, S.R. Sun, Acta Astronautica, 193 (2022).
[10] B.A. Cruden, Journal of Thermophysics and Heat Transfer, 26 (2012).